



Open Archive TOULOUSE Archive Ouverte (OATAO)

OATAO is an open access repository that collects the work of Toulouse researchers and makes it freely available over the web where possible.

This is an author-deposited version published in : <http://oatao.univ-toulouse.fr/>
Eprints ID : 11198

To cite this version : Yang, Chen and Debenest, Gérald Direct numerical simulations for smouldering in horizontal channel. (2013) In: Eighth Mediterranean Combustion Symposium - , 08 September 2013 - 13 September 2013 (Izmir, Turkey)

Any correspondence concerning this service should be sent to the repository administrator: staff-oatao@listes-diff.inp-toulouse.fr

DIRECT NUMERICAL SIMULATIONS FOR SMOULDERING IN THE HORIZONTAL CHANNEL

C. Yang* and G. Debenest

cyang@imft.fr

IMFT, Allée Camille Soula, F-31400 Toulouse, France

Abstract

In the present study, direct numerical simulations for smouldering in a horizontal channel are performed for both compressible and incompressible flows. The reactant gas is passing through the char surface, where the chemical reaction is going to take place. For the sake of simplicity, the smouldering is treated to be a single step chemical reaction. In the incompressible flow, a set of governing parameters are discussed to elucidate their influences on the process of smouldering. Furthermore, the variations of density and dynamic viscosity of gaseous mixture are taken into account in the compressible flow. The comparison between the compressible and incompressible flows reveals that the effects of local compressibility and gaseous mixture on the propagation of smouldering wave are trivial.

Introduction

Smouldering is the flameless combustion of a liquid or solid fuel that derives heat from surface oxidation reactions. In a porous material, the local pore structure allows gaseous reactant to filter through the solid to the reaction site. Substantially, the smouldering wave can propagate through the interior of porous media sample. Due to its vast potential applications, such as porous media burner, waste incineration, catalyst regeneration, oil recovery enhancement and many others applications [1-3], smouldering in porous media has attracted a lot of interests.

In the open literature, tremendous number of publications relevant to the smouldering in porous media can be found. Aldushin et al. [4] started a pioneering work by conducting the one-dimensional theoretical analysis of combustion propagation wave in a porous media. Based on the asymptotic method, structure of solution was determined for the first time. For two different structures, Schult et al. [5] discussed solutions for reaction leading and reaction trailing wave structures by virtue of asymptotic method. A so-called reaction leading structure occurs when the velocity of combustion front overcomes that of the heat transfer layer. On the contrary, the velocity of combustion front is slower than that of the heat transfer layer in the reaction trailing structure.

Regarding to the numerical simulations in the microscope geometry of porous media, two simple structures, which are array of horizontal channels and staggered cylinders, are usually utilized for the computational analysis. Debenest et al. [6] proposed a three-dimensional microscale numerical model for the simulation of smouldering in fixed beds of solid fuels. In light of a dimensional analysis, Debenest et al. [7] identified a set of governing parameters. Furthermore, direct and detailed numerical simulations on the microscale were performed to elucidate their influences.

However, to our best knowledge, no microscale calculations associated with the smouldering in a porous media have been done yet in the compressible flow. In this study, the smouldering in the array of horizontal channels shall be revisited to investigate the effects of a set of governing equations for the incompressible flow. Then, based on the same geometry, we shall consider the variations of density and dynamic viscosity of gaseous mixture to discuss the local effects of compressibility and gaseous mixture in the compressible flow.

Mathematical Model and Governing Equations

As illustrated in Fig 1(a), the gas is passing through the array of horizontal channels. The gray part is the char for combustion, and the other part is the passage for gas. The smouldering, which is simplified to a single step chemical reaction, is going to take place in the interface between these two parts. Due to the periodicity of geometry, a unit cell would be good enough to capture the characteristics of smouldering. Moreover, for the sake of simplicity, the half of a unit cell shown in Fig 1(b) is chosen for the calculations in this study.

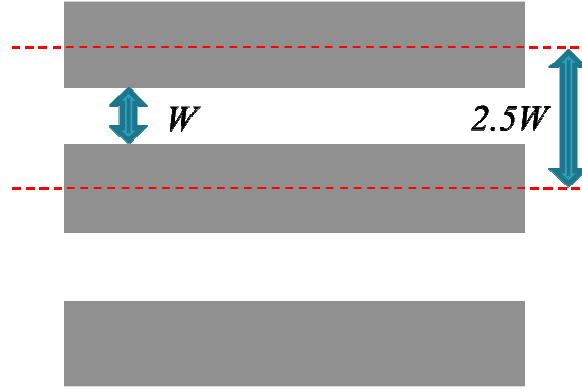


Figure 1(a). Horizontal channels.

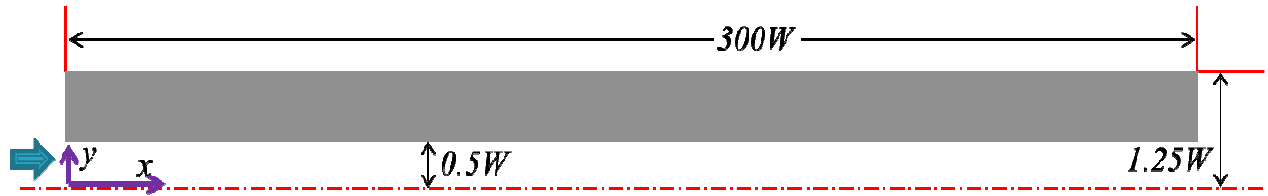


Figure 1(b). Calculation domain.

Based on the mathematical model given by Debenest et al. [6], the governing equations used in this study for incompressible flow are indicated as following:

$$\frac{\partial \rho}{\partial t} + \nabla \cdot (\rho u) = 0 \quad (1)$$

$$\frac{\partial \rho u}{\partial t} + u \cdot \nabla (\rho u) = -\nabla p + \mu \nabla^2 u \quad (2)$$

$$\frac{\partial c_{O_2}}{\partial t} + \nabla \cdot J_{O_2} = 0 \quad (3a)$$

$$J_{O_2} = u c_{O_2} - D_{O_2} \nabla c_{O_2} \quad (3b)$$

$$\frac{\partial (C_g T_g)}{\partial t} + \nabla \cdot J_{T_g} = 0 \quad (4a)$$

$$J_{T_g} = C_g u T_g - \lambda_g \nabla T_g \quad (4b)$$

$$\frac{\partial (C_s T_s)}{\partial t} + \nabla \cdot J_{T_s} = 0 \quad (5a)$$

$$J_{T_s} = -\lambda_s \nabla T_s \quad (5b)$$

where c_{O_2} is the concentration of oxygen, T_g and T_s are the temperature of gas and solid phases, respectively. Moreover, C_g and C_s are the volumetric heat capacities for gas and solid phases.

Correspondingly, the boundary conditions for incompressible flow are set as follows:

For $t = 0$ and inlet:

$$u = u_{in}, T_g = T_s = 500K \text{ and } c_{O_2} = 8.376 \text{ mol}/m^3 \quad (6)$$

For $t = 0$ and outlet:

$$\frac{\partial u}{\partial x} = \frac{\partial T_g}{\partial x} = \frac{\partial T_s}{\partial x} = \frac{\partial c_{O_2}}{\partial x} = 0 \quad (7)$$

Whereas the interfacial conditions between two phases are given by:

$$u = 0 \text{ m/s}, \quad T_g = T_s, \quad \mathbf{n} \cdot (J_{T_g} - J_{T_s}) = \Delta h_c \mathbf{n} \cdot J_{O_2} \quad (8)$$

$$\mathbf{n} \cdot J_{O_2} = S_{O_2} \quad \text{and} \quad \frac{dc_c}{dt} = -\frac{1}{v_g} \int_{\partial v_g} \mathbf{n} \cdot J_{O_2} ds$$

where c_c is the concentration of char, Δh_c is the carbon-oxygen heat of combustion, v_g is the grain volume, ∂v_g is its surface and ds is a surface element.

Furthermore, the properties used in the incompressible flow are listed in Table 1.

Table 1. Properties in the incompressible flow

Solid			Gas		
ρ_s	2100	kg/m^3	ρ_g	0.3	kg/m^3
c_{ps}	800	J/kgK	c_{pg}	1200	J/kgK
λ_s	1	W/mK	λ_g	0.025	W/mK
Δh_c	391.9	kJ/mol	D_{O_2}	2×10^{-4}	m^2/s
			μ	3×10^{-5}	kg/ms

In the incompressible flow, all properties of both gas and solid phases are kept to be uniform and constant. However, in the compressible flow, the variations of density and dynamic viscosity of gas phase are considered in the present study. In addition, the incoming gas is the mixture of oxygen and nitrogen in compressible flow rather than a tracer approximation for oxygen in the incompressible flow. Owing to the utilization of single step chemical reaction, the generation of carbon dioxide is also considered in the compressible flow.

Based on the difference between the compressible and incompressible flows as described above, the governing equations associated with the compressible flow modified from equations (1) ~ (5) are presented as below:

$$\frac{\partial \rho}{\partial t} + \nabla \cdot J_\rho = 0 \quad (9a)$$

$$J_\rho = \rho u \quad (9b)$$

$$\frac{\partial \rho u}{\partial t} + u \cdot \nabla(\rho u) = -\nabla p + \mu \nabla^2 u \quad (10)$$

$$\frac{\partial \rho Y_{O_2} / M_{w_{O_2}}}{\partial t} + \nabla \cdot J_{O_2} = 0 \quad (11a)$$

$$J_{O_2} = (\rho u Y_{O_2} - \rho D_{O_2} \nabla Y_{O_2}) / M_{w_{O_2}} \quad (11b)$$

$$\frac{\partial \rho Y_{CO_2} / M_{w_{CO_2}}}{\partial t} + \nabla \cdot J_{CO_2} = 0 \quad (12a)$$

$$J_{CO_2} = (\rho u Y_{CO_2} - \rho D_{CO_2} \nabla Y_{CO_2}) / M_{w_{CO_2}} \quad (12b)$$

$$Y_{N_2} = 1 - Y_{O_2} - Y_{CO_2} \quad (13)$$

$$\frac{\partial (C_g T_g)}{\partial t} + \nabla \cdot J_{T_g} = 0 \quad (14a)$$

$$J_{T_g} = C_g u T_g - \lambda_g \nabla T_g \quad (14b)$$

$$\frac{\partial (C_s T_s)}{\partial t} + \nabla \cdot J_{T_s} = 0 \quad (15a)$$

$$J_{T_s} = -\lambda_s \nabla T_s \quad (15b)$$

where the Y_i is the mass fraction of pure gas, and the variations of density and dynamic viscosity of gas phase are achieved by the following two equations:

$$\rho = \frac{p}{R_u T_g \sum_{i=1}^N (Y_i / M_{w_i})} \quad (16)$$

and

$$\mu = \sum_{i=1}^N X_i \mu_i \quad (17)$$

where R_u is the universal gas constant, M_{w_i} and X_i are the molecular weight and molar fraction of pure gas, respectively. In addition, μ_i is the dynamic viscosity of pure gas which can be calculated as follows:

$$\mu_i = \frac{AT_g^B}{1 + C/T_g + D/T_g^2} \quad (18)$$

The corresponding coefficients for the pure gas in equation (18) referred from Chapman and Cowling [8] are listed in Table 2.

Table 2. Coefficients in the equation (18)

	A	B	C	D
O_2	1.10×10^{-6}	0.56	96.3	0
CO_2	2.14×10^{-6}	0.46	290	0
N_2	6.56×10^{-7}	0.61	54.7	0

Correspondingly, the boundary conditions for compressible flow are set as follows:

For $t = 0$ and inlet:

$$u = u_{in}, T_g = T_s = 500K, Y_{O_2} = 0.8935, 0.1787, 0.0596, Y_{CO_2} = 0, Y_{N_2} = 1 - Y_{O_2} - Y_{CO_2} \quad (19)$$

For $t = 0$ and outlet:

$$\frac{\partial u}{\partial x} = \frac{\partial T_g}{\partial x} = \frac{\partial T_s}{\partial x} = \frac{\partial Y_{O_2}}{\partial x} = \frac{\partial Y_{N_2}}{\partial x} = \frac{\partial Y_{CO_2}}{\partial x} = 0 \quad (20)$$

Whereas the interfacial conditions between two phases are given by:

$$u = 0 \text{ m/s}, \quad T_g = T_s, \quad \mathbf{n} \cdot (J_{T_g} - J_{T_s}) = \Delta h_c \mathbf{n} \cdot J_{O_2}, \quad \mathbf{n} \cdot J_{O_2} = S_{O_2}, \quad (21)$$

$$\mathbf{n} \cdot J_{CO_2} = S_{CO_2} = S_{O_2} \times M_{w_{CO_2}} / M_{w_{O_2}}, \quad \mathbf{n} \cdot J_\rho = S_\rho = S_{CO_2} - S_{O_2} \frac{dc_c}{dt} = -\frac{1}{v_g} \int \mathbf{n} \cdot J_{O_2} ds$$

In the present study, a set of governing parameters used for the analysis are presented as follows:

$$Pe = \frac{u_B W}{D_o}, \quad \Delta = \frac{C_g \Delta c_c}{C_s \Delta c_{O_2}}, \quad T_{ad} = \frac{\varepsilon_s \Delta c_c \Delta h_c}{\varepsilon_g C_g + \varepsilon_s C_s}, \quad T_p = \frac{T_{ad}}{|\Delta - 1|} \quad (22a, b, c, d)$$

where ε_g and ε_s are porosities of gas and solid phases, T_{ad} and T_p are the adiabatic temperature and plateau temperature, respectively.

Code Validations

The foregoing sets of governing equations are solved numerically by using the OpenFOAM Version 2.1.1 package. Since the process of smouldering is transient, PIMPLE algorithm designed for the large time-step computations is chosen to be the numerical scheme. The transient terms of the foregoing sets of governing equations were discretized using the first order Euler implicit scheme. For the convergence criteria, the residuals of all variables are less than 10^{-12} . Moreover, we have performed a sensitivity analysis to the grid size. Then, all of the calculation results in the present study are independent of the grid size.

As depicted in Fig 2., the fully developed velocity profile of cross-section in the channel is compared with the corresponding exact solution. It can be seen that the agreement between two velocity profiles is good. According to the prediction of Debenest et al. [7], the transversally averaged temperature is supposed to reach the plateau temperature calculated by equation (22d). In Fig. 3., the transversally averaged temperature comes to the plateau temperature when the location of combustion front is 70W.

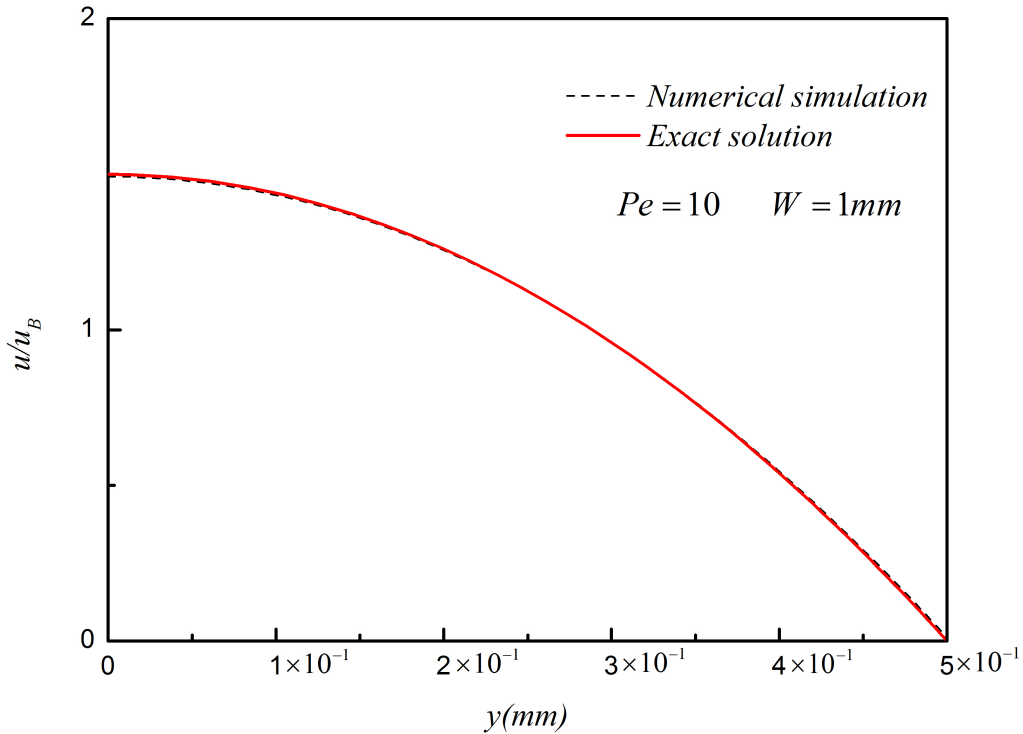


Figure 2. Comparison of fully developed velocity profile in a channel with the exact solution

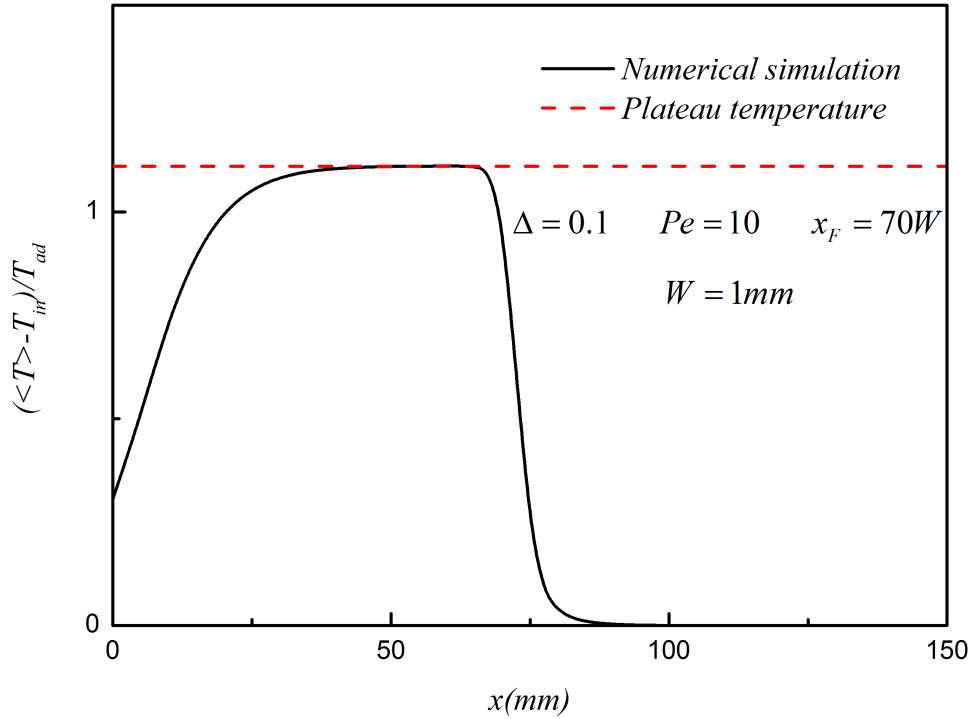


Figure 3. Profile of the transversally averaged temperature in the horizontal channel

Results and Discussion

Several tests were made in order to check the accuracy of the model. They are all summarized in Table 3.

For all the calculations, Pe and Δ , we report in Table 3 are the results obtained for averaged temperature divided by the adiabatic one. If the results are correct, it will normally converge to the value of $1/|\Delta - 1|$, according to Aldushin et al. [4]. We can see a good agreement with the theory for $Pe = 1, 10$; $\Delta = 0.1$ with a profile of averaged temperature coming to the expected temperature. But, for Δ values equal to 0.5 and 1.5, less than 3% of difference is observed. This is the asymptotic value reached numerically and several things could explain that. Main direction we have today, is the grid size in y direction as the reaction term depends strongly on the concentration of oxygen. This will be investigated in a forthcoming paper. But as evidence, we can consider that the numerical tool is valid, and could be a starting point for further investigations. We are now going to see more in details of the results.

As illustrated in Fig 4., Fig 5. and Fig6., profiles of transversally averaged temperature of gas and solid phases are presented for three different Δ . The Peclet number, Pe , is kept constant and equal to 10. Different Δ can be interpreted as different char concentration in the solid or different oxidizer concentration in the gas. In these three figures, it can be clearly seen that the smouldering wave propagates as the time goes by, and eventually comes to the steady regime. This time depends on the flow regime as seen in Debenest et al. [7].

Table 3. Several cases in the present study

$Pe \backslash \Delta$	0.1		0.5		1.5	
	T_p/T_{ad}					
	Numerical	Analytical	Numerical	Analytical	Numerical	Analytical
1	1.11	1.111		2.0		2.0
10	1.11	1.111	1.976	2.0	1.97	2.0

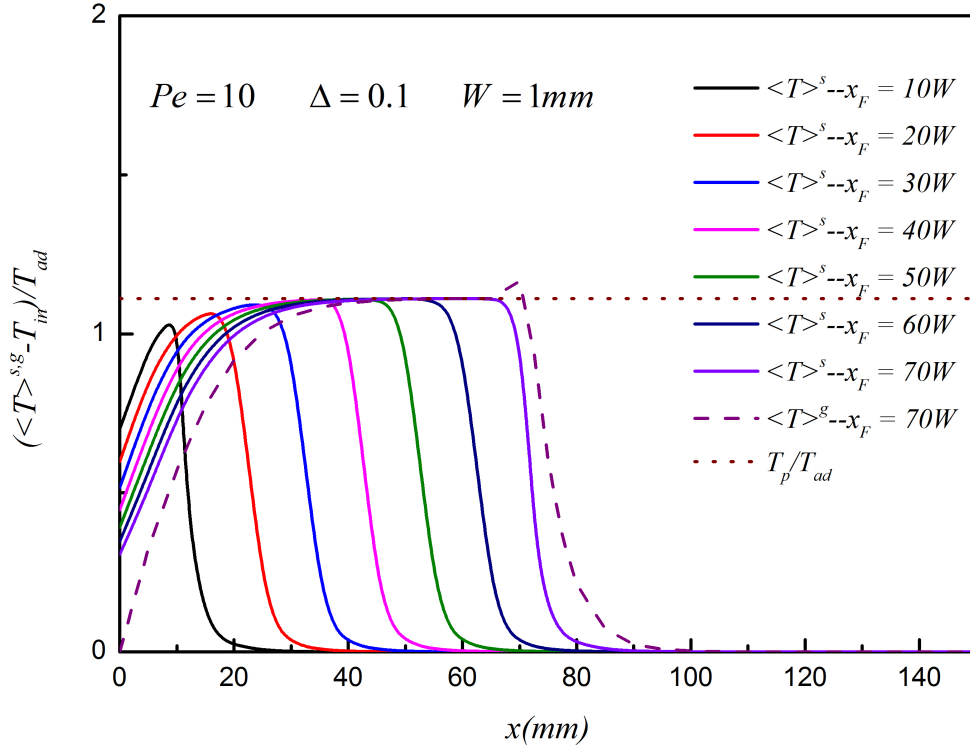


Figure 4. Profiles of the transversally averaged temperature of fluid and solid phases for $\Delta = 0.1$ and $Pe = 10$ in incompressible flow.

In the Fig. 4., the steady regime is obtained after 40 W. We can see a difference in the averaged temperature profiles between gas and solid phase. At the inlet, the gas phase needs several W before being at the equilibrium with the solid phase. A peak is observed in the gas phase, in the reaction region. Then, the gas phase appears to be hotter than the solid phase. This is due to the convective part in the equation (4a).

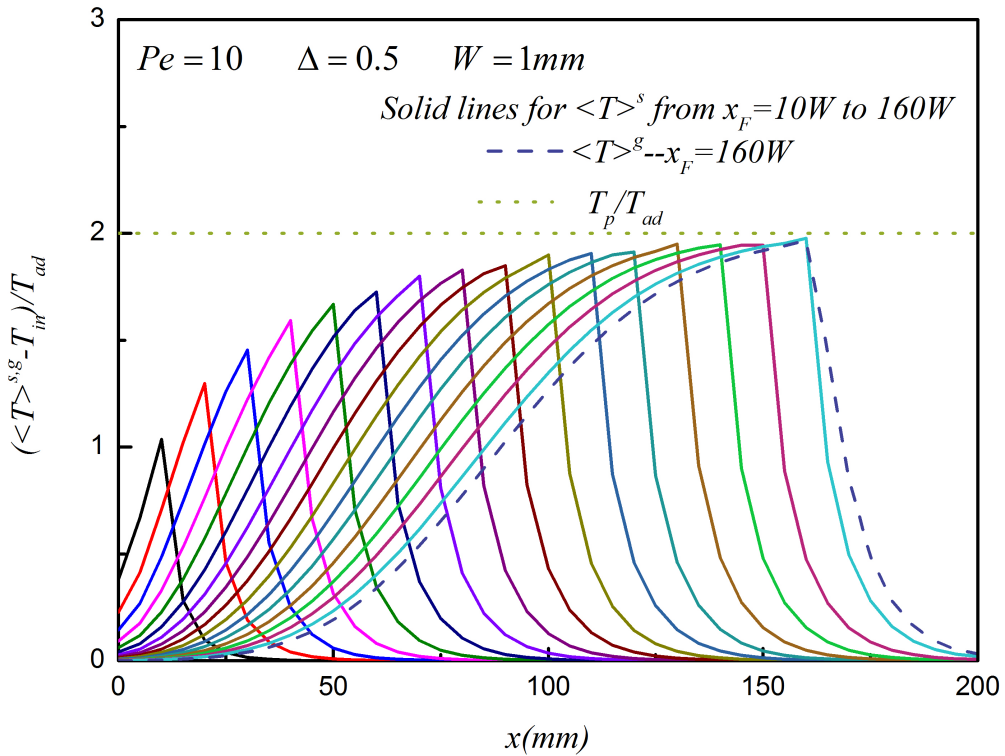


Figure 5. Profiles of the transversally averaged temperature of fluid and solid phases for $\Delta = 0.5$ and $Pe = 10$ in incompressible flow.

In the Fig. 5., the steady regime is obtained after 160 W. The maximum averaged temperature is really closed to the one expected. We also observe that the heat content stays closer to the reaction region than in the previous case. This is coming from the increasing Δ value. Heat velocity is now closed to the reaction front velocity and the two waves propagate at nearly the same speed.

In the figure 6, the steady regime is obtained after 220W. The maximum temperature is closed to $2T_{ad}$. The thermal wave propagates quicker than the reaction wave, so the heat content accumulates after the reaction region.

In these last two cases, we see the same differences in averaged profiles between gas and solid phases than in figure 4. The convective part of equation (4a) explains once again this effect comment could be done. This is in agreement with the results of Debenest et al. [7]. But we present there the first local approach reaching the steady regime expected.

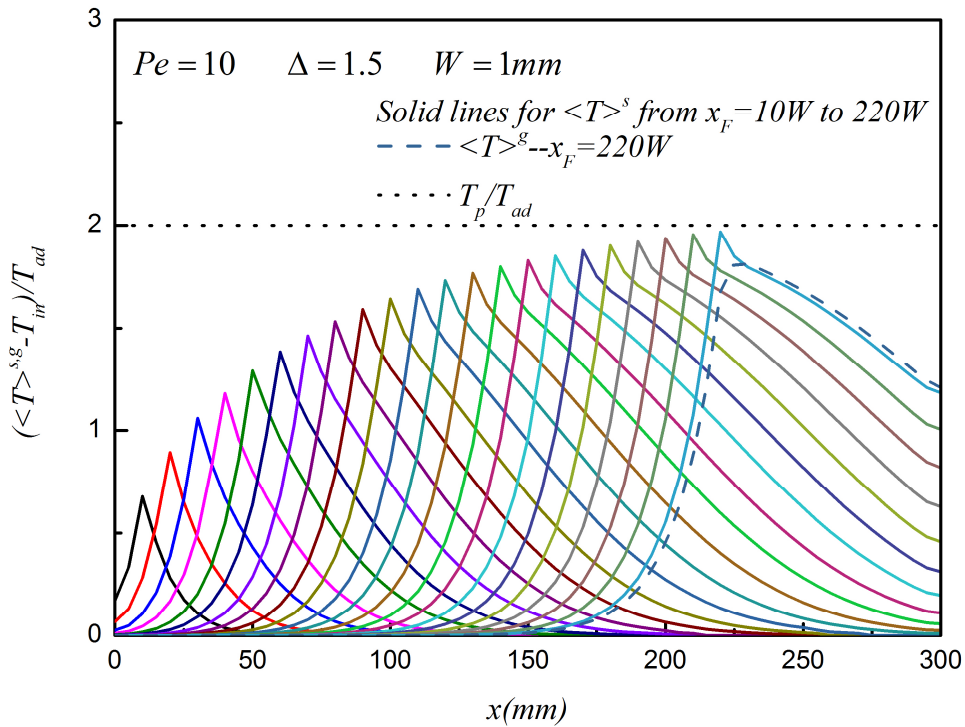


Figure 6. Profiles of the transversally averaged temperature of fluid and solid phases for $\Delta = 1.5$ and $Pe = 10$ in incompressible flow.

In Fig. 7, the case $Pe = 1$; $\Delta = 0.1$ is given. After 50W, the steady regime is observed and the averaged temperature reaches the expected value. When the combustion front comes to 70W, the averaged profiles of gas temperature and solid temperature are plotted. No significant differences exist, except in the inlet zone, where the gas phase enters at 500K. In the front region, a peak temperature exists in the gas phase. This comes from the reaction at the interface. Then, the gas temperature releases to the solid temperature. The same Δ value with a $Pe = 10$, gives us a strong difference in space between the two temperatures. Because of the small value of Pe and especially of thermal Pe value like explained in Debenest et al. [9], in this case no differences are seen.

Let's go now to the compressible flows as introduced in equation (9) to (15). The last part of this paper will be dedicated to the comparison between incompressible and compressible flows and quantification of the effects of composition and temperature with density and dynamic viscosity. Several tests will be made to compare with our incompressible case by varying Pe number, intensive and further investigation of Δ values will be addressed in a coming paper.

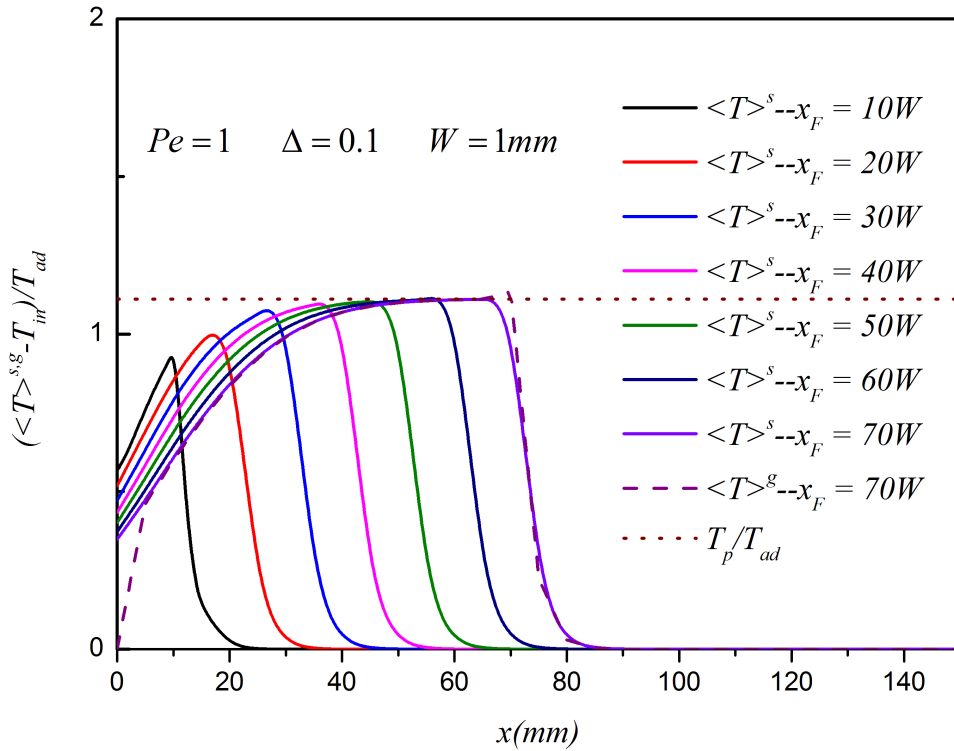


Figure 7. Profiles of the transversally averaged temperature of fluid and solid phases for $\Delta = 0.1$ and $Pe = 1$ in incompressible flow.

In the Fig. 8 and Fig. 9, the cases of $Pe = 1$ and 10 for the $\Delta = 0.1$ are presented in the compressible flow. By comparing these two figures with Fig. 4. and Fig. 7, it can be seen that the variations of density and dynamic viscosity of gas phase have no remarkable influences on the propagation of smouldering wave. The further investigations seem to be necessary, such as more accurate chemical reaction schemes, variation of thermal capacity of gas phase, etc.

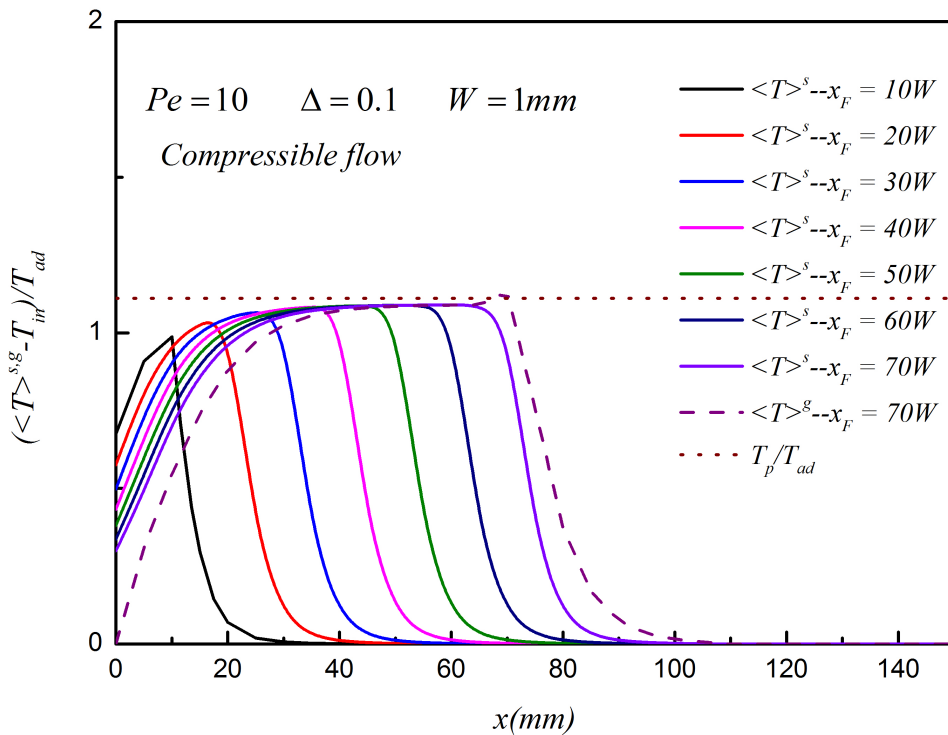


Figure 8. Profiles of the transversally averaged temperature of fluid and solid phases for $\Delta = 0.1$ and $Pe = 10$ in compressible flow.

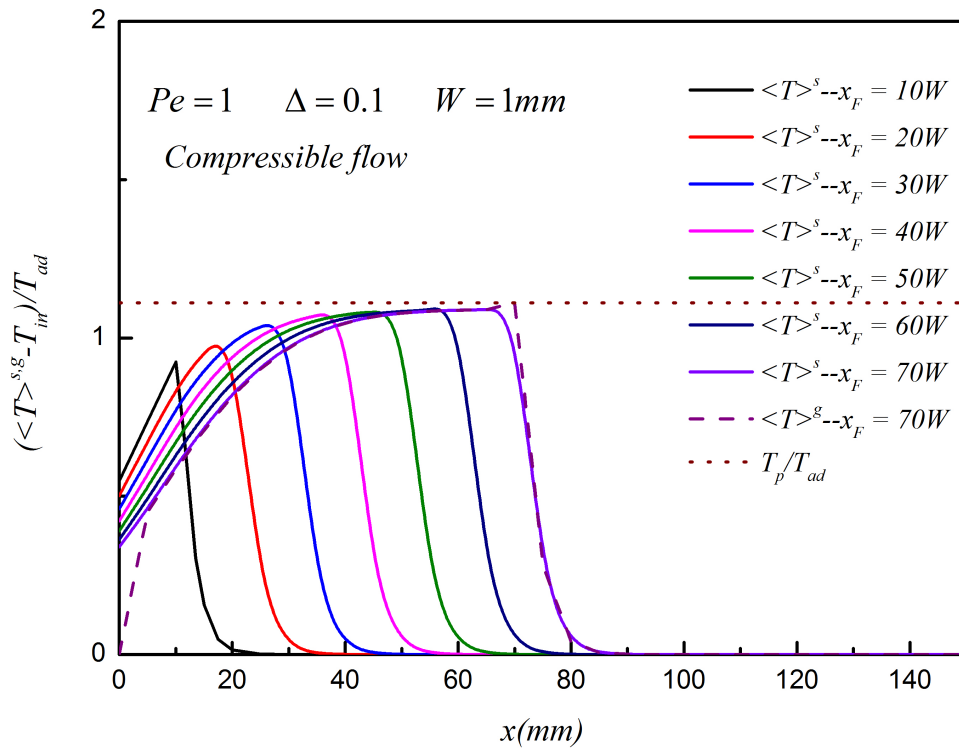


Figure 9. Profiles of the transversally averaged temperature of fluid and solid phases for $\Delta = 0.1$ and $Pe = 1$ in compressible flow.

As shown in the Fig. 10 and Fig. 11, the difference of pressure, density and dynamic viscosity of gas phase between the compressible and incompressible flows are plotted in the direction of smouldering wave propagation. The comparison results clearly indicate that the difference is significant; especially in the chemical reaction region. This is because the variations of density and dynamic viscosity of gas phase are highly temperature-dependent.

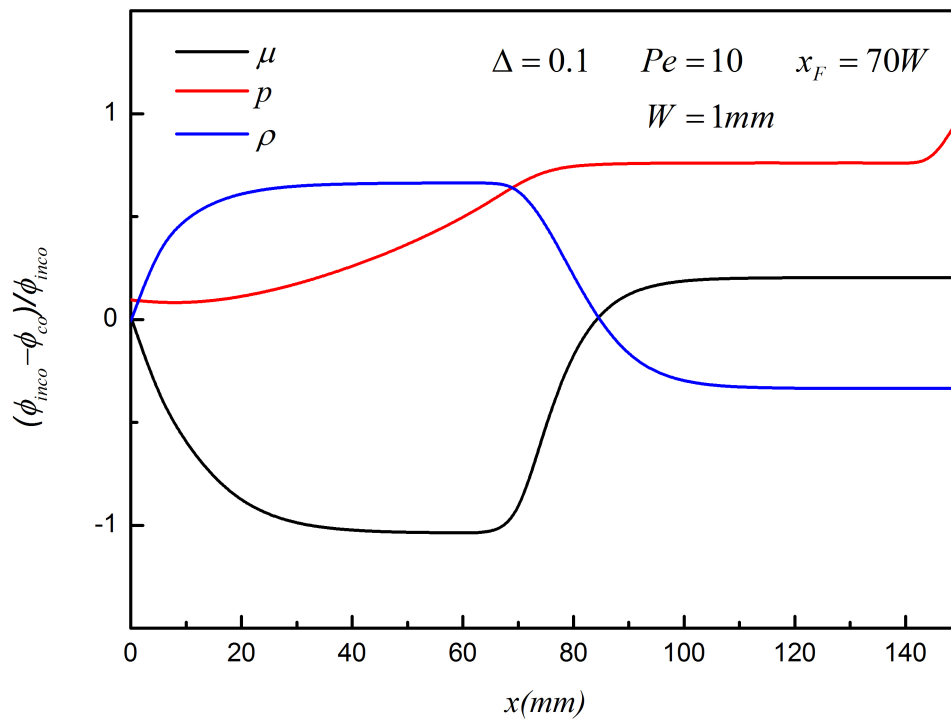


Figure 10. Comparisons between the compressible and incompressible flows for $\Delta = 0.1$ and $Pe = 10$

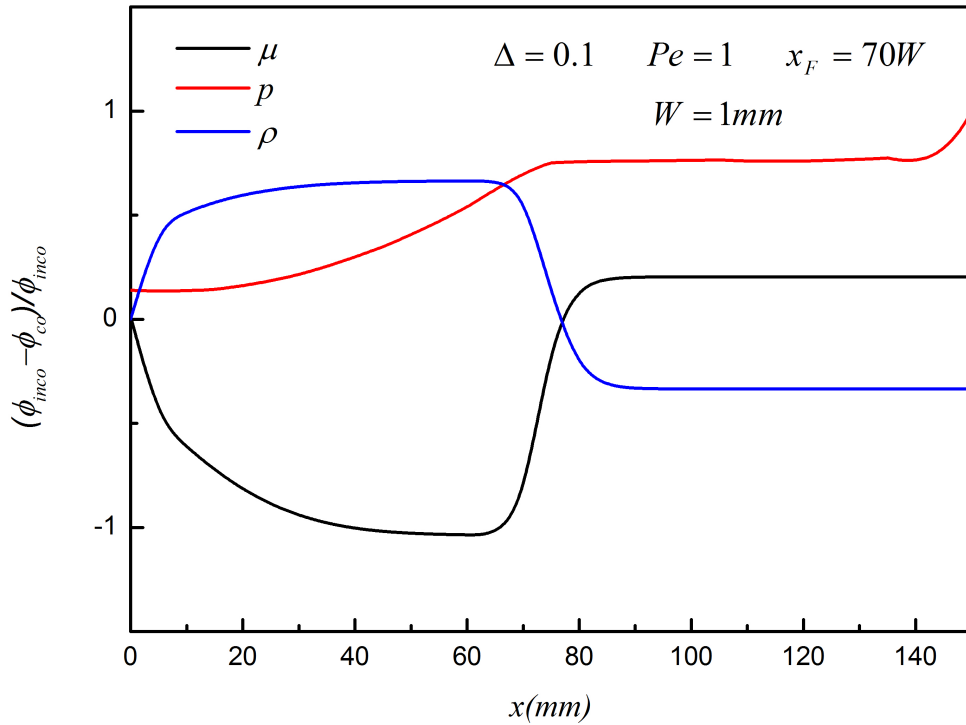


Figure 11. Comparisons between the compressible and incompressible flows for $\Delta = 0.1$ and $Pe = 1$

Conclusions

In the present study, direct numerical simulations were made to investigate the effects of a set of governing parameters on the smouldering process in a horizontal channel. The calculations were carried out for both compressible and incompressible flows. In the incompressible flow, it was found that a so-called reacting leading structure appears for $\Delta < 1$, and $\Delta > 1$ results in the reacting trailing structure. Moreover, it also should be noted that for the same Δ , the case of $Pe = 1$ has smaller temperature difference between the gas and solid phases than that of $Pe = 10$ does, which implies that the local thermal equilibrium assumption could be valid in the case of $Pe = 1$. By varying the density and dynamic viscosity of gas phase, the calculations were conducted in the compressible flow to discuss the effects of local compressibility and gaseous mixture on the propagation of smouldering wave. The comparison between the compressible and incompressible flows demonstrates that the variations of pressure, density and dynamic viscosity of gas phase in the direction of smouldering propagation wave are significant. However, the effects of local compressibility and gaseous mixture on the propagation of smouldering wave are negligible.

Nomenclature

c	concentration
C	volumetric heat capacity
D	diffusivity of pure gas
h_c	carbon-oxygen heat of combustion
J	flux
M_W	molecular weight
p	pressure
Pe	Pelect number
R_u	universal gas constant
S	source term

T	temperature
u	velocity
W	height of gas passage
x, y	Cartesian coordinates
X	molar fraction
Y	mass fraction
ε	porosity
λ	thermal conductivity
μ	dynamic viscosity
ρ	density

Subscripts

ad	adiabatic
c	char
B	bulk
F	combustion front
g	gas
in	inlet
O_2	oxygen
N_2	nitrogen
CO_2	carbon dioxide
p	plateau
s	solid

Superscripts

g	gas
s	solid

References

- [1] Sarathi, P. S., *In-situ combustion handbook—principles and practices*, Tulsa, 1999.
- [2] Ohlemiller, T. J., “Modeling of smouldering combustion propagation”, *Prog. Energy Comb. Sci.* 11: 277-310 (1985)
- [3] Oliveira, M., Kaviany, M., “Nonequilibrium in the transport of heat and reactants in combustion in porous media”, *Prog. Energy Comb. Sci.* 27: 523-545 (2001)
- [4] Aldushin, A. P., Merzhanov, A. G., Seplyarskii, B. S., “Theory of filtration combustion of metals”, *Fiz Goren Vzryua* 12: 323-328 (1976)
- [5] Schult, D. A., Matkowsky, B. J., Volpert, V. A., “Forced forward smolder combustion”, *Eng. Sci.* 2180: 1-26 (1996)
- [6] Debenest, G., Mourzenko, V., Thovert, J. F., “Smouldering in fixed beds of oil shale grains: a three-dimensional microscale numerical model”, *Comb. Theory and Modelling*, 9: 113-135 (2005)
- [7] Debenest, G., Mourzenko, V., Thovert, J. F., “Smouldering in fixed beds of oil shale grains: governing parameters and global regimes”, *Comb. Theory and Modelling*, 9: 301-321 (2005)
- [8] Chapman, S., Cowling, T., *The mathematical theory of non-uniform gases*, Cambridge University Press, 1939.
- [9] Debenest, G., Mourzenko, V., Thovert, J. F., “Three-dimensional microscale numerical simulation of smoldering process in heterogeneous porous media”, *Comb. Sci. and Tech.* 180: 2170-2185 (2008)